Propagation of short fatigue cracks from notches in a Ni base superalloy: experiments and modelling

F. SANSOZ[1] B. BRETHES[2] and A. PINEAU[1]

[1]*Centre des Materiaux, UMR 7633 CNRS, Ecole des Mines de Paris, Evry cedex, France,* [2]*SNECMA, service YKOM, Etablissement de Villaroche, Moissy Cramayel, France*

Received in final form 11 June 2001

ABSTRACT A notched specimen containing a semicircular slot (0.1 mm deep) was designed to simulate the growth of three-dimensional short cracks under a stress concentration. Fatigue tests were performed on N18 superalloy at 650 °C with trapezoidal loading cycles. A high-resolution optical measurement technique proved to be capable of detecting half-surface crack increments as small as 10 μm, and the potential drop method was found to be inappropriate for very small crack lengths. The stress intensity factor, ΔK, was calculated using a weight functions method. Non-uniform stress fields were determined by FEM modelling using elasto-viscoplastic constitutive equations. The plasticity-induced crack closure effect was calculated within the specimen using viscoplastic FEM modelling. The prediction of crack aspect ratio was used to investigate differences of closure along the crack front. The role of notch plasticity on these differences is discussed. Using these calculations, it is shown that the apparent differences between the growth behaviour of short and long cracks can be largely accounted for.

Keywords crack closure; finite element calculations; short fatigue cracks; three-dimensional effects.

NOMENCLATURE

a = semi-elliptical crack depth
a_0 = initial crack depth
c = half surface crack length
a/c = crack aspect ratio
Ci, Di = coefficients in the kinematic hardening law ($i = 1, 2$)
E = Young's modulus
F = LEFM geometry shape factor
K = stress intensity factor
K_{op} = stress intensity factor when the crack is fully opened
p = cumulated plastic strain
Q, b = coefficients in the isotropic hardening law
R = load ratio ($= S_{min}/S_{max}$)
R_{eq} = equivalent semicircular crack radius in PD technique
S = applied load divided by the reduced section of specimen
S_{max} = maximum applied load divided by the reduced section of specimen
S_{min} = minimum applied load divided by the reduced section of specimen
S_{op} = crack opening applied load divided by the reduced section of specimen
t = specimen thickness
U = crack closure coefficient ($= \Delta K_{eff}/\Delta K$)

Correspondence: A. Pineau, Centre des Materiaux, UMR 7633 CNRS, Ecole des Mines de Paris B.P. 87, 91003 Evry cedex, France.
E-mail: pineau@mat.ensmp.fr

U_A = crack closure coefficient calculated within the specimen
U_C = crack closure coefficient calculated at the free surface of the specimen
V_f = volume fraction
α, K, n = coefficients in the Norton creep law
δa = crack depth increment
δc = half surface crack length increment
$\Delta\varepsilon_p$ = plastic strain range
ΔK = stress intensity range ($= K_{max} - K_{min}$)
ΔK^* = corrected stress intensity range
ΔK_A = stress intensity range given within the specimen
ΔK_C = stress intensity range given at the free surface of the specimen
ΔK_{eff} = effective stress intensity factor range ($= K_{max} - K_{op}$)
$\Delta K_{eff,A}$ = effective stress intensity range given within the specimen
$\Delta K_{eff,C}$ = effective stress intensity range given at the free surface of the specimen
$\Delta\sigma$ = local stress range ($= \sigma_{max} - \sigma_{min}$) in the vicinity of the notch root
ν = Poisson's ratio
σ = local stress in the vicinity of the notch root

INTRODUCTION

N18 alloy is a Ni base superalloy used to build advanced turbine discs for aircraft engines. This alloy is obtained by powder metallurgy (PM) and can accidentally contain an extremely small amount of inclusions due to the fabrication process. The typical size of the biggest microstructural defects is no more than 100 μm but, under the stress concentration located at turbine blades fixtures, small elliptical fatigue cracks ($\geqslant 0.1$ mm) could eventually be initiated. Moreover, due to high applied loads and elevated temperatures, non-uniform stress fields are developed in the vicinity of notches. It is therefore very important to investigate the growth behaviour of these short fatigue cracks considering notch plasticity effects.

The behaviour of physically small cracks (<0.5 mm) as defined by Suresh and Ritchie,[1] has been mainly studied on unnotched specimens. Pearson[2] and Lankford[3] carried out the first experiments showing anomalous short crack growth rates below the conventional crack growth threshold obtained on long cracks (>0.5 mm). Then a number of authors, in particular Minakawa *et al.*[4] and Journet *et al.*,[5] developed the concept of intrinsic threshold to correlate the differences observed between short and long cracks. In this approach, it is considered that the range of applied load is smaller than the stress intensity range, $\Delta K = K_{max} - K_{min}$, and is equal to $\Delta K_{eff} = K_{max} - K_{op}$, where K_{op} is the stress intensity factor calculated when the crack is fully opened. Therefore, an explanation of the typical short crack behaviour was directly related to the calculations of the effective stress intensity range ΔK_{eff} linked to crack closure effects[6] which are, in this case, strongly dependent of the crack length. Smith and Miller[7] investigated the behaviour of physically small cracks emanating from notches. Due to the notch plasticity effect, the load applied far from the notch can not be directly used and a local approach must be considered to determine the stresses. This approach was used successfully in several studies[8–11] in which crack closure effects were shown to significantly reduce the crack growth rates differences observed between short and long cracks. More recently Pommier *et al.*[12,13] have tested N18 alloy at 650 °C. These authors concluded that the stress relaxation effects occurring at elevated temperature at the notch root can largely modify the effective stress intensity factor ΔK_{eff} when the crack is small in length (<0.5 mm). On Rene 95 alloy, Van Stone *et al.*[14] suggested a methodology involving both the notch plasticity and typical three-dimensional (3D) effects on fatigue crack growth rates observed for the in-depth and the surface growth of penny-shaped cracks. However limitations were found both to obtaining accurate measurements of very small surface crack growth rates from notches at high temperatures and to calculation of the effective stress intensity factor for semi-elliptical cracks under inelastic stress gradients.

The aims of the present study were therefore: (1) to propose an approach to extend the previous studies of the behaviour of semi-elliptical short cracks emanating from notches at high temperature, considering recent approaches to ΔK calculations;[15,16] and (2) to show that the linear elastic fracture mechanics can be validated under creep–fatigue loading to correlate crack growth rates using an appropriate calculation of ΔK_{eff} as a function of the length and the shape of the crack.

MATERIAL AND EXPERIMENTAL PROCEDURE

All tests were carried out on a 'bulk' microstructure of N18 alloy.[17] The chemical composition of this material was: 11.5% Cr-15.7% Co-6.5% Mo-4.35% Al-4.35% Ti-0.5% Hf, balance Ni (weight %). After annealing treatment at 1165 °C for 4 h, N18 alloy was found to contain a population of coarse γ' precipitates (≈ 5 μm) with a volume fraction (V_f) of 15%, which was sufficient to control the grain size (10–20 μm). After air cooling, a second population of smaller γ' precipitates (≈ 0.3 μm) was formed in the grains ($V_f \approx 45\%$). The size, shape and distribution of these precipitates depend on cooling rates. Two ageing treatments at 700 and 800 °C were then applied for 24 and 4 h, respectively. Given this treatment, the N18 alloy displayed not only a high mechanical strength but also excellent fatigue and creep resistance up to 650 °C. The monotonic and cyclic yield stresses at 650 °C were equal to 1050 and 1150 MPa, respectively. For a more comprehensive overview on this alloy, see Refs [17,18].

The growth rates of long cracks were obtained on conventional unnotched specimens with a thickness of 2.5 mm (KB2.5) containing a semicircular electro-discharged machined (EDM) defect of 0.3 mm in depth. This geometry is represented in Fig. 1(a). Precracking was carried out at room temperature with a loading frequency of 10 Hz to obtain a semicircular crack with a depth of 0.5 mm. Fatigue crack growth tests were performed on this geometry at the temperature of use in turbine discs (650 °C) and at a lower temperature (450 °C) using a radiation furnace. Two thermocouples welded on the back face of the specimen were used to monitor the temperature, which was controlled to ± 2 °C. The load ratio $R = S_{min}/S_{max}$ was kept equal to 0.1 or 0.3. Typical trapezoidal cycles 10 s–300 s–10 s with a hold time of 5 min at maximum nominal load were applied. Triangular continuous cycles at low frequency (10 s–10 s) were also used. The crack growth rate was measured on these specimens for crack lengths up to 2 mm in depth using a conventional potential drop technique and a calibration procedure.[19]

A geometry with two symmetrical U-shaped notches (DEN) was specifically designed to study the effect of a stress gradient on the behaviour of short cracks. The notch root radius was 2 mm and the reduced cross-section was 5 mm–10 mm [Fig. 1(b)]. A microstructural defect was simulated by a small semicircular EDM slot of 0.1 mm in depth located at the centre of the notch root on one side of the specimen. This machined defect is shown in Fig. 1(c). It can be seen that the thickness of the EDM slot in the KB2.5 and DEN specimens were different. In KB2.5 specimens, the slot thickness was not important as crack growth rates were measured only after relatively large crack extension (≈ 0.2 mm). Preliminary tests with a square-shaped slot showed that stepwise cracks were initiated. This explains why a sharp notch was adopted for these specimens. In DEN specimens, the thickness of the slot was kept as small as possible (50 μm) to develop a planar crack from the notch. No precracking was made on the DEN specimens and the crack length on the free surface of the specimen was measured up to 1 mm from the initial semicircular defect (0.1 mm). Tests were performed only at 650 °C with trapezoidal cycles 10 s–300 s–10 s. These specimens were tested with a constant nominal maximum stress S_{max} varying from 600 to 900 MPa, which represent, respectively, 0.5 and 0.8 times the monotonic yield strength, and load ratios equal to 0, -0.5 or -1. Great attention was paid to avoiding any buckling or bending moment when the specimen was loaded in compression.

Two techniques were developed to measure the growth of a semi-elliptical crack in these notched specimens. First, data were obtained from a direct current potential drop (PD) system in which a 6 A pulsed current was applied. In order to make the PD method sensitive enough, 0.1 mm diameter probe wires were spot welded across the EDM notch. Due to the small size of the EDM defects, the probe wires were kept sufficiently away from the machined defect to prevent cracks from being initiated from the welding points. This location is represented in Fig. 1(b). An equivalent crack length is obtained from a calibration method, in which a semi-elliptical crack is approximated as a semicircular crack (see insert of Fig. 3) with a radius R_{eq}, which is calculated as $(R_{eq})^2 = a \cdot c$, where a and c are crack depth and half surface crack length, respectively.

Moreover a far-field optical microscope was used to measure crack lengths at the free surface of the specimen in the notch bottom. The specimen was observed through a window machined in the wall of the radiation furnace. The image was monitored and the crack length was measured using a sight-slit. This technique has proved to be efficient to detect *in situ* half surface crack increments as small as 10 μm.

RESULTS

Long crack growth rates

Figure 2 presents the crack growth rate measured on KB2.5 unnotched specimens using the stress intensity factor calculated in depth of the crack, ΔK_A, with Newman–Raju equations.[20] These results were obtained with a stress ratio, R, equal to 0.30, i.e. in the absence of any crack closure effect since it was previously shown that, in this material, K_{op} for long cracks is close to 0.24 K_{max}.[21] Fig. 2 shows that higher fatigue crack growth rates were obtained when a hold time of 5 min was

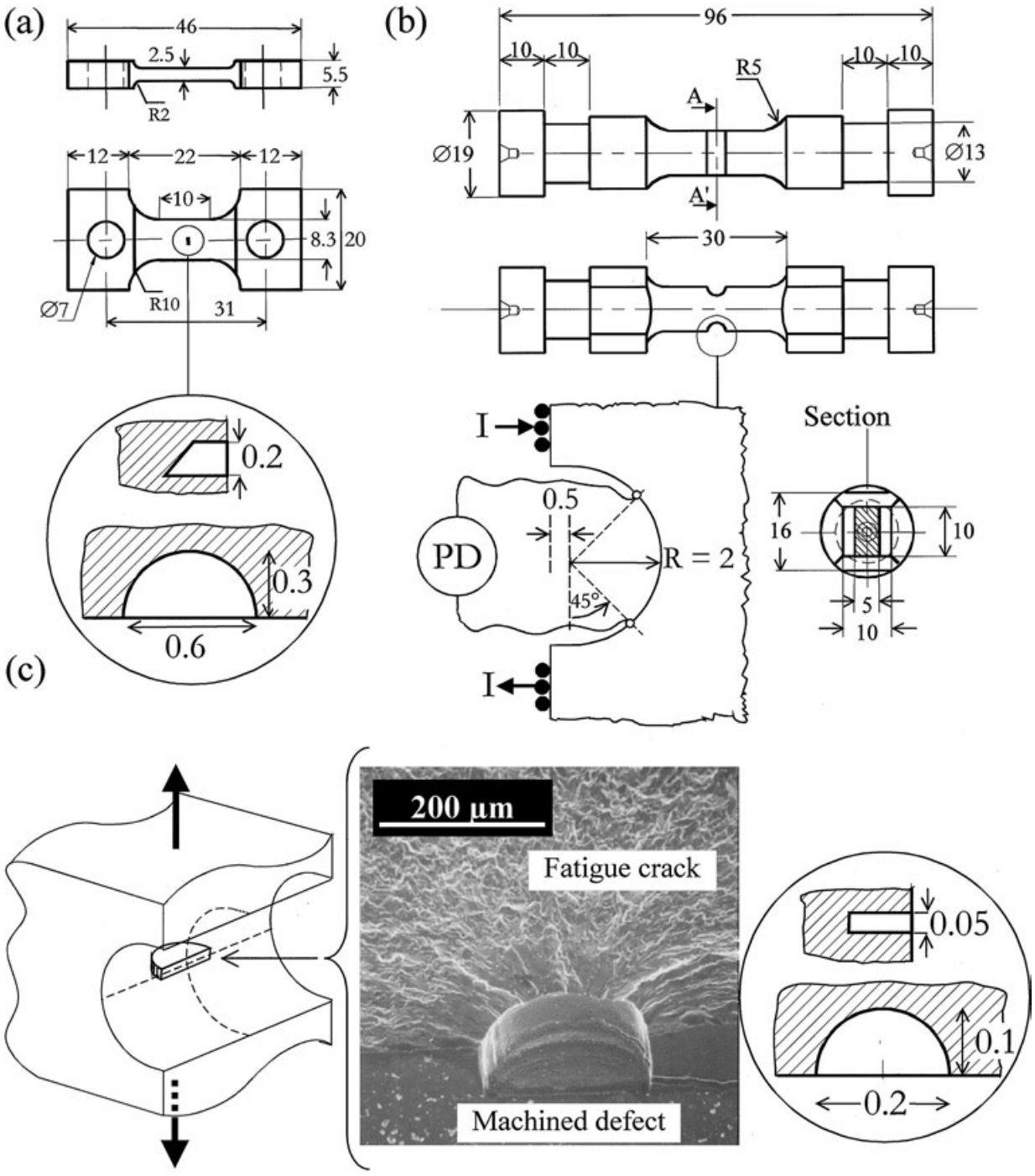

Fig. 1 Geometry of fatigue crack growth specimens used in this study. (a) Unnotched specimen (KB2.5) for the growth of semi-elliptical long cracks. (b) Double-edge-notched specimen (DEN) for the growth of semi-elliptical short cracks and location of electrodes used for PD measurements. (c) Semi-circular initial defect. All dimensions are given in mm.

imposed during the cycle as compared to a continuous loading (cycles 10 s–10 s). Moreover, a change in fracture mode from an intergranular crack path with cycles 10 s–300 s–10 s to transgranular with cycles 10 s–10 s was observed as has been shown elsewhere.[17,18] These authors showed that, in the N18 alloy, the hold-time effect on crack propagation was a combination of both environmental effects related to intergranular oxidation-assisted embrittlement and creep strains due to stress relaxation taking place during the hold time. At the

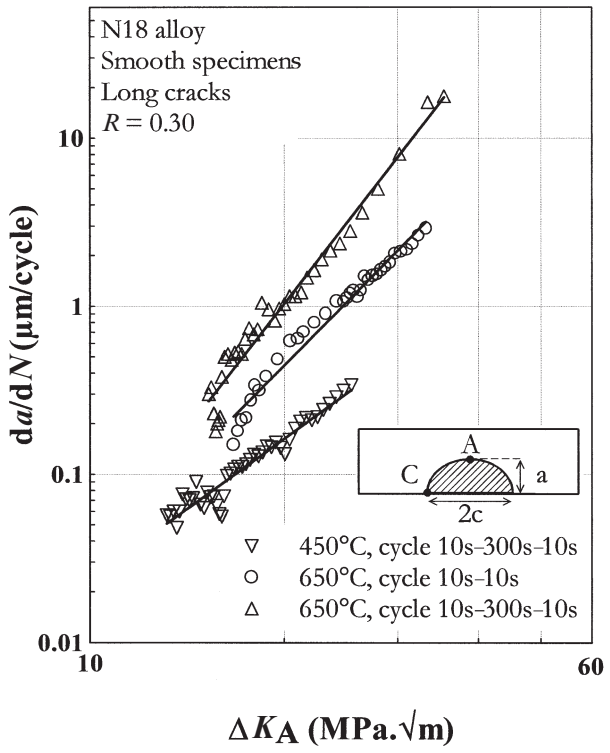

Fig. 2 Results of long crack growth rate measurements in N18 alloy tested at elevated temperature (450 and 650 °C).

lower temperature (450 °C) where the environmental effects are less predominant, lower crack growth rates associated with transgranular fracture mode were obtained with 10 s–300 s–10 s cycles. It can be concluded from the fracture modes observed in the present study on KB2.5 specimens that environmental effects are very similar to those observed in compact tension specimens ($a > 10$ mm).[17,18]

Short crack growth rates

Typical results obtained on notched specimens with $S_{max} = 700$ MPa and $R = 0$ are shown in Fig. 3. In this figure, both equivalent crack depths from the PD technique and optical surface crack measurements are presented. In all tests, half surface crack length increments were observed from the first cycles. On the contrary, the first deviation of the PD technique occurred only when surface crack lengths reached about 300 µm. A rather good agreement between both measurement techniques was only observed for surface crack lengths larger than 400 µm. Small differences observed in this range of crack lengths may be due to the assumption made regarding the crack shape defined by the crack aspect ratio *a/c*. As shown later, *a/c* was less than 1 for short cracks and slightly larger than 1 for larger cracks. Figure 3 shows that, for a test duration of 4423 cycles, the PD method was inappropriate for more than one-half of the test duration (≈2500 cycles) to detect the growth of very small cracks (<400 µm). In the following, only the results obtained by optical measurements are presented.

The measured short crack growth rates are plotted for different applied loads in Fig. 4. Two stages of crack propagation were observed with the tests performed at $R = 0$ [Fig. 4(a)]. The first stage corresponded to decreasing rates when surface crack lengths were less than 200 µm and then above this critical crack length, a steady increase in growth rates. The downward trend of the crack growth rate curves or short crack effect was more pronounced for a low applied load, S_{max}, of 600 MPa. For this load, the arrow in Fig. 4(a) represents a crack growth rate less than 10^{-8} m/cycle occurring during the crack propagation. Moreover it was observed that lowering the R ratio from 0 to −1 overcame the downward trend effect [Fig. 4(b)]. These results show the significance of notch plasticity effects on crack growth behaviour.

In comparison with the measurements made by Pommier *et al.*[12,13] on N18 alloy with the same DEN geometry, a difference of one order of magnitude in crack growth rates was observed [Fig. 4(c)]. The size of small γ' precipitates was, however, larger in the bulk microstructure used in the present study [Fig. 5(a)] than that tested by Pommier *et al.* [Fig. 5(b)]. As shown in Refs [17,18] the significant difference in crack growth behaviour is directly related to the size of secondary γ' precipitates. It has been shown that the stress relaxation, which plays a key role in time-dependent fracture micromechanisms, was largely dependent of the size of these γ' precipitates.

MODELLING AND DISCUSSION

ΔK calculations

The stress intensity range, ΔK, was calculated using the weight functions method introduced by Wang and Lambert,[15,16] which was established for semi-elliptical cracks under non-uniform stress gradients. The local stress–strain field near the notch in the absence of a crack was calculated by finite element method (FEM). ZéBuLoN FEM code developed by the Ecole des Mines de Paris was used for this purpose. A two-dimensional (2D) mesh with plane strain elements represented one-quarter uncracked DEN specimen. Refined meshing (≈25 µm) with quadratic elements was used in the vicinity of the notch root to model stress and strain gradients. The material behaviour was represented using an elasto-viscoplastic constitutive set of equations proposed by Lemaitre and Chaboche:[22]

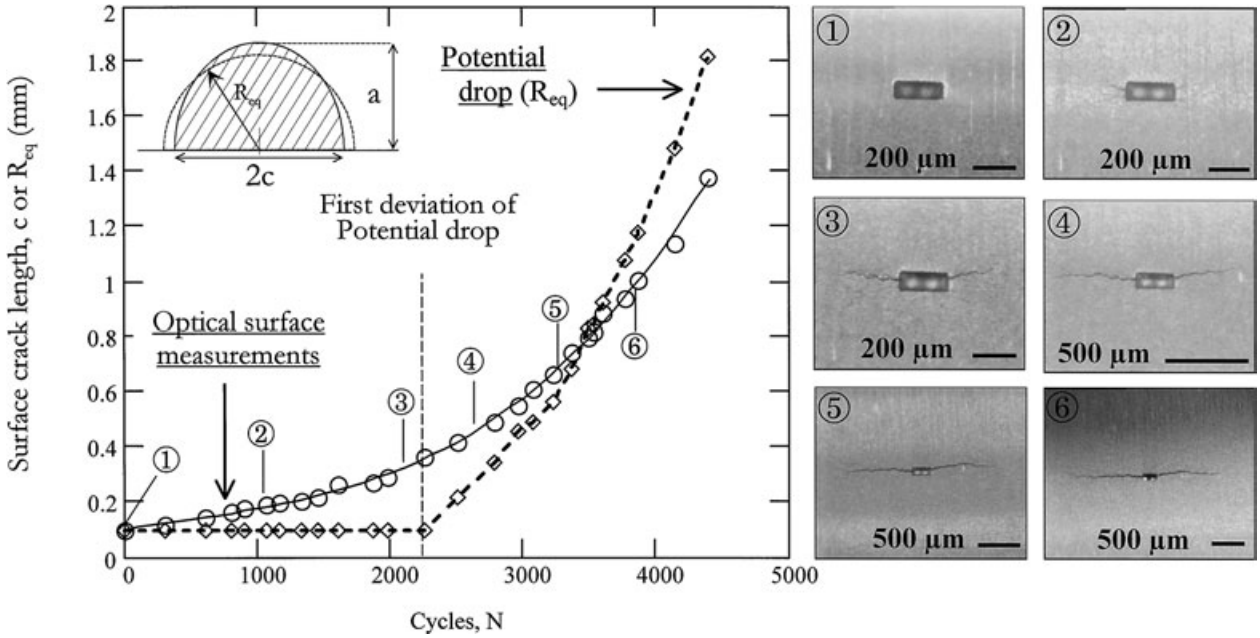

Fig. 3 Typical short crack growth measurements with high-resolution optical technique and potential drop method.

Elastic constants:

$E = 170\,000$ MPa; $\nu = 0.25$

Isotropic hardening:

$$R = R_0 + Q[1 - \exp(-b \cdot p)] \tag{1}$$

with the cumulated plastic strain,

$$p = \int_0^t \sqrt{\frac{2}{3}\dot{\varepsilon}_p(\tau) : \dot{\varepsilon}(\tau)}\, d\tau \tag{2}$$

Kinematic hardening:

$$\dot{\tilde{X}} = \sum_{i=1}^{2} \dot{\tilde{X}}_i \quad \text{with } \dot{\tilde{X}}_i = \frac{2}{3} C_i \dot{\tilde{\varepsilon}}_p - D_i \cdot \dot{p} \cdot \tilde{X}_i \tag{3}$$

Creep law:

$$\dot{p} = \left\langle \frac{f}{K} \right\rangle^n \cdot \exp\left[\alpha \cdot \left\langle \frac{f}{K} \right\rangle^{n+1} \right] \tag{4}$$

where

$$f = \mathcal{J}_{II}(\tilde{\sigma} - \tilde{X}) - R \tag{5}$$

with

$$\mathcal{J}_{II} = (\tilde{\sigma} - \tilde{X}) = \sqrt{\frac{3}{2}(\tilde{s} - \tilde{X}') : (\tilde{s} - \tilde{X}')} \tag{6}$$

In these equations, the coefficients (R_0, Q, b, C_i, D_i, K, n and α) were identified using low-cycle fatigue tests performed at 650 °C.[23] These coefficients are shown in Table 1.

Detailed results of FEM calculations at the notch root with cyclic loading are given in references.[23,24] These FEM calculations showed that the tensile stress ahead of the notch progressively decreased to reach a stabilized condition, which was obtained after about 50 creep–fatigue cycles. Stabilized profiles at $R = 0$ with different applied loads are presented in Fig. 6(a). As expected, significant compressive stresses were noticed when the specimen was unloaded. This led to an increase of the local applied stress range at the notch root. A simple correction to calculate ΔK accounting for the cyclic plasticity at the notch root was used, as proposed by Haigh and Skelton.[25] In this approach, the equivalent stress intensity range, ΔK^*, was calculated as:

$$\Delta K^* = (U \cdot \Delta\sigma + E \cdot \Delta\varepsilon_p) \cdot \sqrt{(\pi a)} \cdot F \tag{7}$$

where F is the LEFM geometry shape factor given by $F = \Delta K/[\Delta\sigma \cdot \sqrt{(\pi a)}]$, $\Delta\sigma$ is the total portion of the local stress range, U is the crack closure coefficient ($U = \Delta K_{eff}/\Delta K$), E is the Young's modulus and $\Delta\varepsilon_p$ is the plastic strain range in the vicinity of the notch. The pseudo-elastic stress, $E \cdot \Delta\varepsilon_p$, calculated from stabilized profiles is represented in Fig. 6(b) for different applied loads. For moderate applied stress ranges (<900 MPa), the strain range remains predominantly elastic. In this case, the calculated pseudo-elastic stress, $E \cdot \Delta\varepsilon_p$, is less than 100 MPa. But for higher applied stress ranges ($R = -1$; $S_{max} = 600$ MPa), $E \cdot \Delta\varepsilon_p$ can be larger than 200 MPa. However, the correction on ΔK given by Eq. (7) is less than 10% for this range when the crack depth is more than 90 µm. These calculations suggest that an elastic approach in terms of ΔK should apply in

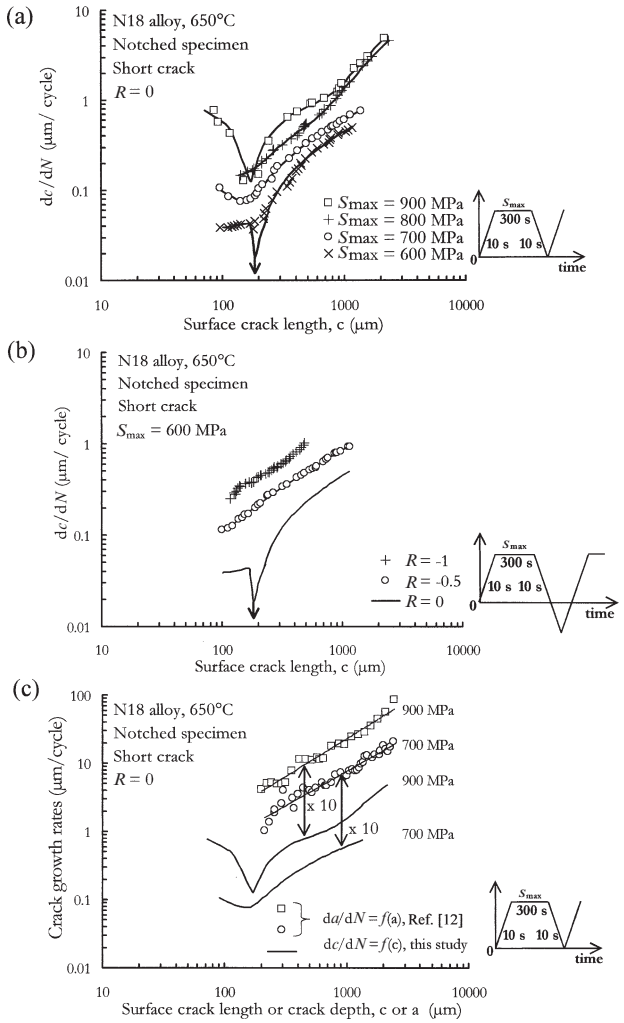

Fig. 4 Short crack growth rates measured in DEN notched specimens (N18 alloy at 650 °C). (a) Effect of maximum applied stress at $R = 0$. (b) Effect of mean stress. (c) Comparison with Refs [12,13].

this situation. Stress profiles at S_{max} and S_{min} similar to those shown in Fig. 6(a) were approximated by a polynomial expression used in Wang and Lambert's results[15,16] to calculate both K_{max} and K_{min}. The results, which were used to compare the crack growth rates measured both on short cracks and on long cracks, are shown in the following section.

Crack-closure modelling and ΔK_{eff} calculations

In order to compare the crack growth rates of notched and unnotched specimens, the effective stress intensity factor, ΔK_{eff}, corresponding to these geometries must be determined first. In the present work, only plasticity-induced crack closure mechanisms will be considered. In this fine-grain material, other closure mechanisms, notably those related to oxide and surface roughness, are

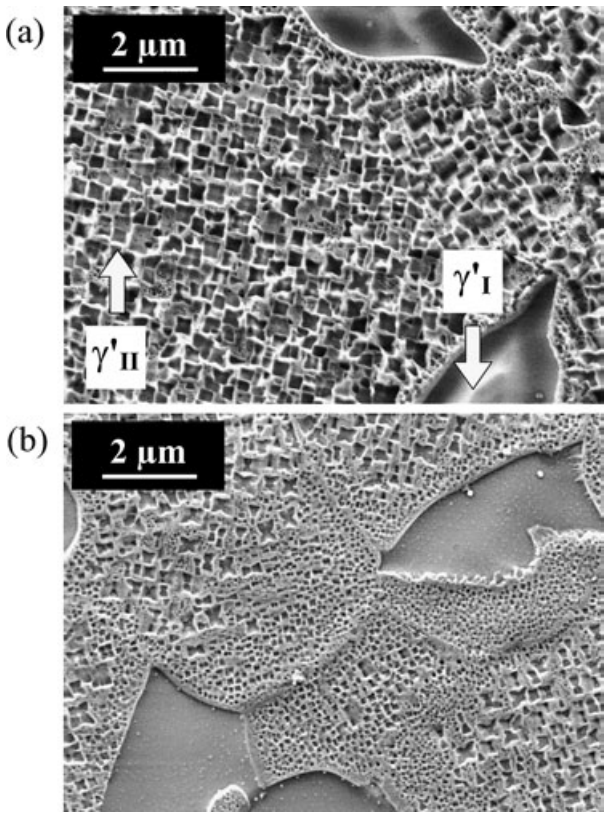

Fig. 5 Microstructural differences observed in N18 alloy. (a) Microstructure used in this study. (b) Microstructure used by Pommier *et al.*[12,13]

Table 1 Coefficients of viscoplastic constitutive equations identified on N18 alloy at 650 °C. For kinematic hardening the values of C_i/D_i ratios corresponding to stabilized regime are given

Isotropic hardening law	Kinematic hardening law	Creep law
$R_0 = 87$ MPa	$C_1/D_1 = 326.5$	$n = 4.4$, $K = 9750$
$Q = 111$, $b = 3$	$C_2/D_2 = 215.5$	$\alpha = 30\,000000$

assumed less significant. For unnotched specimens containing a semicircular crack, the crack closure effects are generally more pronounced near the surface than along the crack front within the specimen.[26–29] This difference could be explained by the loss of constraint near the surface.[29] Most of the related data in the literature are obtained from studies employing 3D FEM calculations, which are exhaustive in nature, particularly when considering notched bodies coupled with viscoplastic material response. To overcome these difficulties, the current study utilized a simplified 2D FEM model to calculate the crack closure at the crack depth (point A in Fig. 2). The results of this model were then used in a 3D analytical simulation in order to calculate closure effects

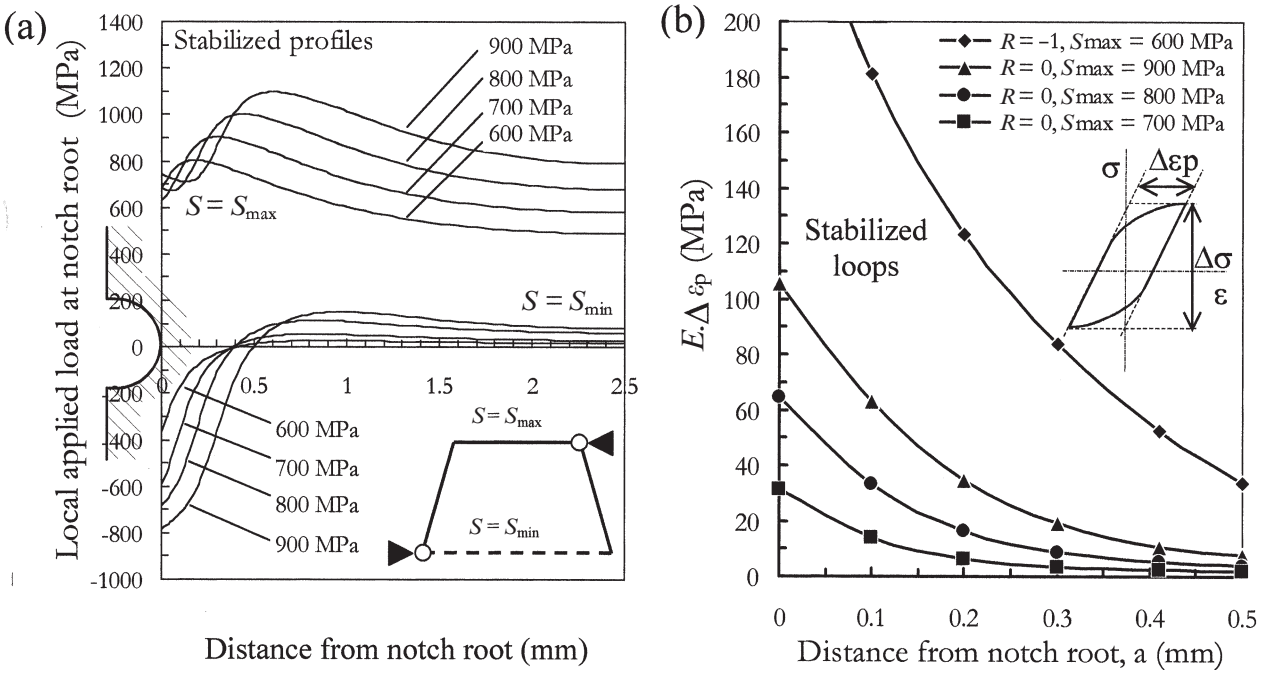

Fig. 6 Stabilized stress and strain gradients calculated in the vicinity of the notch. Effect of applied loading (a) on local stress at maximum load (S_{max}) and minimum load (S_{min}) and (b) on pseudo-elastic stress calculated from plastic strain range.

at the surface points of the crack. Both the 2D FEM model and the 3D analytical method will be explained in this section.

The 2D FEM model is based on a node-release technique similar to that proposed by Newman and Armen,[30] which was used to simulate the growth of a fatigue crack in a 2D mesh. This technique was performed using ZéBuLoN code in which the viscoplastic constitutive Eqs (1)–(6) were applied to calculate the stress gradients in a notched specimen. Plane strain conditions were assumed within the specimen. The mesh of a half-notched DEN specimen was compared with the unnotched geometry as shown in Fig. 7(c). In both meshes [Fig. 7(a) and (b), respectively], the propagation area was refined with eight-node quadratic elements (Fig. 7(c). The size of the smallest element in this area is 20 μm. Crack propagation is simulated from 0.095 to 1 mm measured from the free surface. In this analysis, the release of one node corresponds to three loading cycles (10 s–300 s–10 s). Nodes are released at the minimum load level. Details of this numerical procedure are given elsewhere.[12,13,23,31]

This model calculates the crack opening ratio S_{op}/S_{max} of a 2D crack propagating in a notched specimen subjected to different applied loads and R ratios; see Fig. 8(a). The opening load S_{op} was numerically determined by examining the load–displacement curve of the node closest to the crack tip. On this curve, a sharp change in slope was easily detected when the load reached S_{op}. The initial crack length, a_0, is equal to the depth of the machined EDM slot (0.10 mm). In this figure, it is seen that for all load conditions, the crack opening ratio is small in the vicinity of the notch. This ratio increases with increasing crack length and reaches a stable maximum value ($S_{op}/S_{max} \approx 0.2$) at a crack depth of 300–400 μm. This stabilized value is approximately the same for all loading conditions. The profile of the crack opening ratio as obtained from this 2D model is assumed in this study, to be similar to that experienced by the in-depth point along a 3D semi-elliptical crack.

On the basis of this assumption, a procedure was established to determine the opening stress intensity factor, K_{op}, of a semi-elliptical crack under a stress gradient. This procedure is described as follows. For a stress level equal to S_{op}, the stabilized stress profile at the notch root in a specimen without a crack is determined. The corresponding K_{op} is then calculated using Wang and Lambert's weight functions given at the deepest point of the crack front (point A in Fig. 2). Figure 8(b) shows the results of this procedure for $S_{max} =$ 700 MPa and $R = 0$ for a semicircular crack front ($a/c =$ 1). It is observed that the numerical results obtained on unnotched specimens are in good agreement with the experimental data for long cracks, as given in Ref. [21] ($K_{op} = 0.24\,K_{max}$). Furthermore, the opening ratios between unnotched and notched specimens are very similar when the crack is long (>200 μm). However, the crack closure effect is significantly less pronounced with

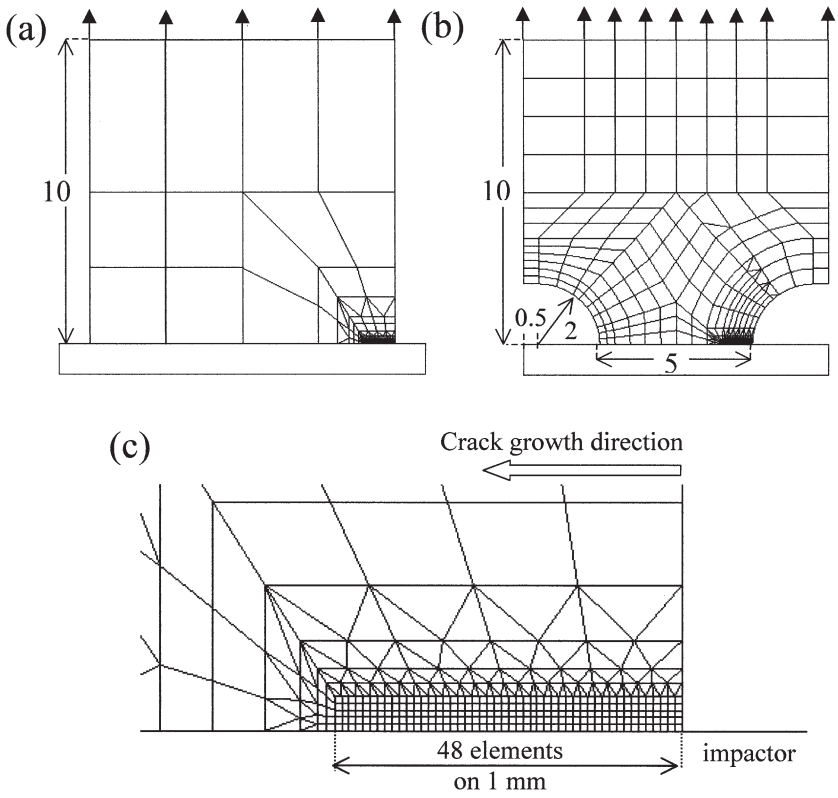

Fig. 7 Crack growth simulated by node release scheme. (a) In unnotched mesh. (b) In DEN notched mesh. (c) Refined mesh for crack propagation in both specimens.

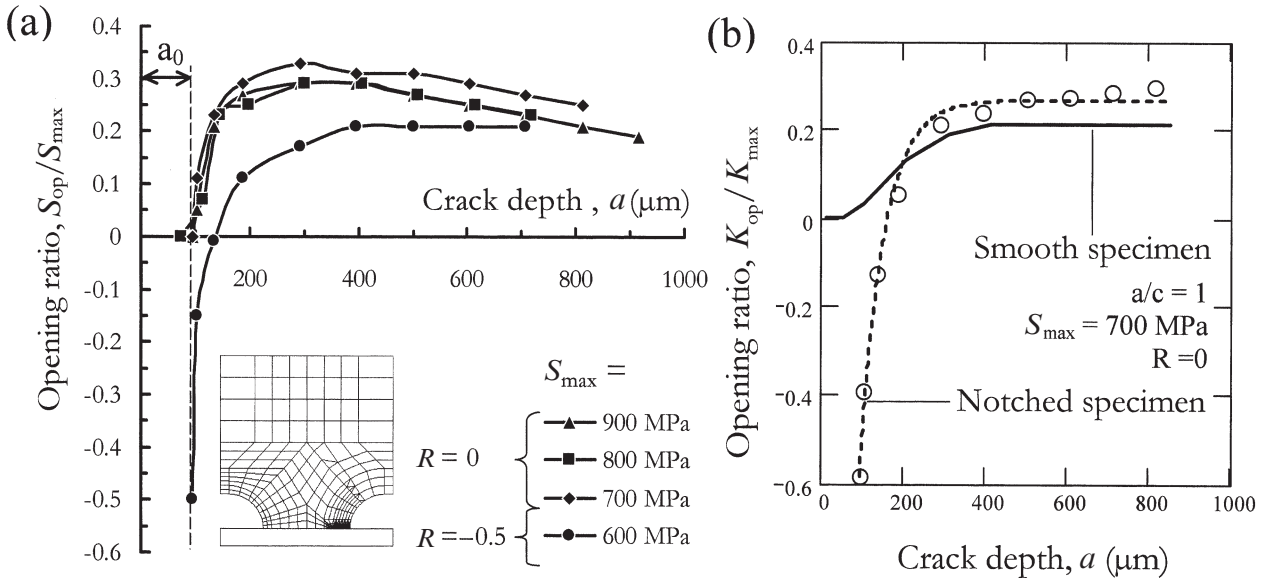

Fig. 8 Crack opening ratios calculated by FEM method. (a) S_{op}/S_{max} ratio. (b) K_{op}/K_{max} ratio.

notched specimens when the crack is very small (<200 μm). This result is in agreement with those obtained by Pommier *et al.*[13]

The crack closure at the free surface (point C in Fig. 2) was estimated from the knowledge of the opening ratios inside the specimens and using the method proposed by Jolles and Tortoriello.[32] In this technique, the crack growth increments at A and C, δa and δc, respectively, are correlated as follows:

$$\delta a = \left(\frac{\Delta K_{\text{eff,A}}}{\Delta K_{\text{eff,C}}}\right)^n \times \delta c = \left(\frac{U_A \Delta K_A}{U_C \Delta K_C}\right)^n \times \delta c \qquad (8)$$

where n is the Paris law exponent ($n = 4.871$ in N18

alloy at 650 °C[23]), U_A and U_C are the crack closure coefficients given at A and C, respectively. The method consists of the prediction of the crack aspect ratio, *a*/*c*, calculated iteratively from Eq. (8) imposing the shape of the initial defect. Figure 9 represents typical results obtained on DEN specimens tested with $S_{max} = 900$ MPa and $R = 0$. The analysis of the crack front shape obtained from interrupted tests as shown in Fig. 9(a) indicates that the use of the ratio $U_C/U_A = 1$ is not a valid assumption; see Fig. 9(b). A correction to this approach was the use of a procedure introduced by Jolles and Tortoriello,[32] which is applied to fit the ratio U_C/U_A using experimental measurements of the crack front shape, as shown in Fig. 9(b). The ratio used in this figure is fitted into the form:

$$\frac{U_C}{U_A} = 0.55 + (1 - 0.55) \cdot \exp\left[-2 \cdot \frac{a - a_0}{t} \right] \quad (9)$$

where t is the thickness of the specimen ($t = 5$ mm) and a_0 is the initial crack depth. This result shows that crack closure effects are more important along the free surface than inside the specimen. Jolles and Tortoriello[32] reached similar conclusions from observations on unnotched specimens ($U_C/U_A = 0.91$). It can, however, be noticed that the difference in crack closure along the crack front is less significant in unnotched specimens than in notched ones. The difference between these two geometries can be related to the increase of local stress range in the vicinity of the notch. Further studies to validate Eq. (9) for different applied loads are necessary. In the present work, the effective stress intensity factor in C, $\Delta K_{eff,C}$, was calculated using Eq. (9) for notched DEN specimens and $U_C/U_A = 0.9$ for unnotched specimens.

Crack growth rate analysis

The crack growth rates obtained from notched specimens tested at 650 °C are shown in Fig. 10. This figure includes the results for long cracks obtained on conventional CT type specimens.[24] It also includes relatively long crack data obtained in this study using unnotched KB2.5 specimens (Fig. 2).

In Fig. 10(a), where no crack closure effect is considered, short and long cracks exhibit significant differences in crack growth behaviour at the free surface (point C), particularly at high ΔK values. It is also observed that a decreasing d*a*/d*N* pattern is present at low values of ΔK. Similar results are obtained for in-depth crack growth rates (point A). In this case, to calculate ΔK at point A (ΔK_A), it was assumed that $a/c = 1$, which is in good agreement with the experimental results shown in Fig. 9, at least when half surface crack lengths reached approximately 1 mm. It could then be assumed that $da/dN \approx dc/dN$. Figure 10(b) shows both the fatigue crack growth rates d*c*/d*N* versus $\Delta K_{eff,C}$ at point C and d*a*/d*N* versus $\Delta K_{eff,A}$ at point A. In this figure, it is observed that the short crack growth rates effects found in notched specimens at lower values of

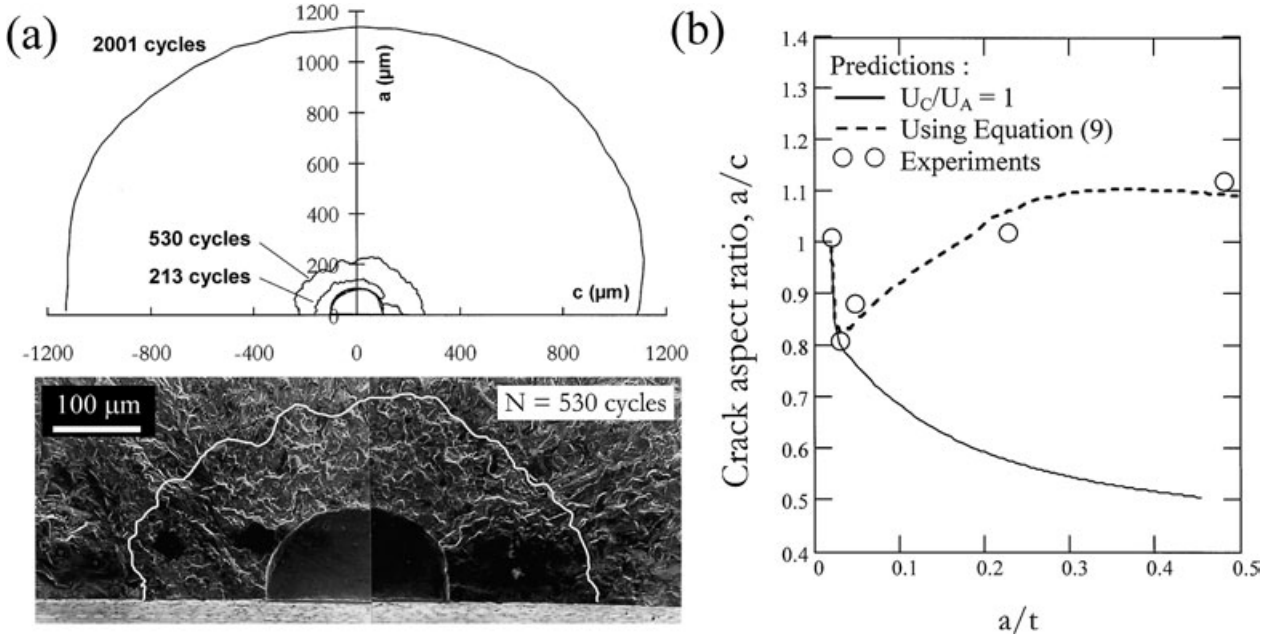

Fig. 9 Crack aspect ratio analysis involving 3D crack closure effects. (a) Experimental observations of crack front in notched specimens tested at 650 °C with $R = 0$ and $S_{max} = 900$ MPa. (b) Numerical predictions.

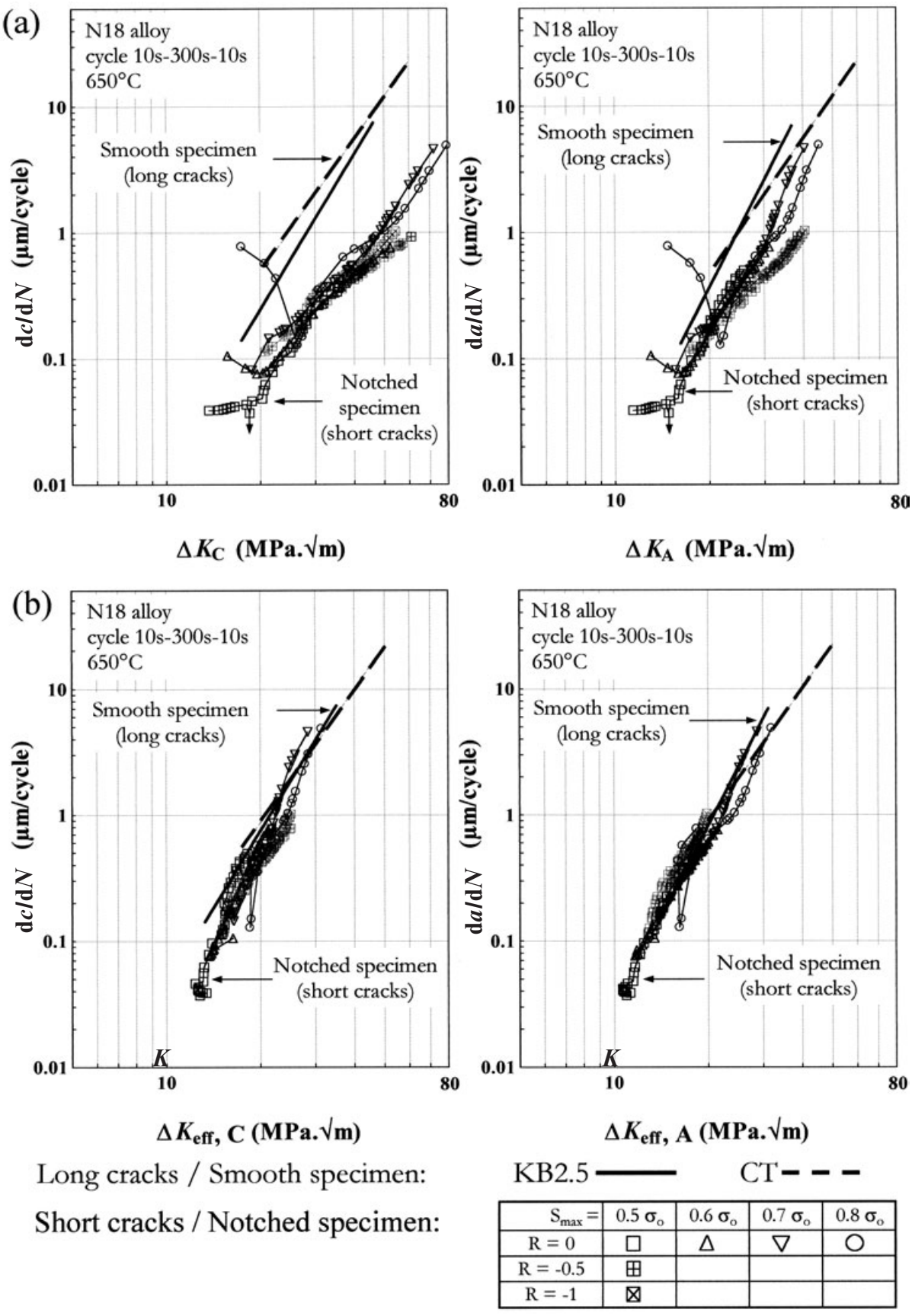

Fig. 10 Comparison of fatigue crack growth rates measured in unnotched and notched specimens. Both free surface and in-depth measurements are given. (a) No crack closure effect is considered. (b) 3D crack closure effects are considered.

ΔK no longer exist when closure effects are properly taken into account.

Another way of presenting these results is to calculate the life spent to propagate a crack over a given distance using experimental results similar to those shown in Fig. 3. In this specific case, it is found that the number of cycles calculated to grow a crack of 1380 μm in length using the methodology previously developed, is 3472 cycles, which is very close to the experimental data (4423 cycles). A simplified engineering method would consider only the positive range of loading by means of K_{max} parameter calculated from stabilized viscoplastic profiles with a semicircular crack shape. Calculations showed that K_{max} is significantly higher than ΔK_{eff} in Fig. 3 except when the crack is only less than 200 μm in depth. However, the predicted value obtained with this parameter represents more than 13 600 cycles. This comparison emphasizes the significance in lifetime calculations of taking the very early stage of crack propagation into account.

CONCLUSIONS

Accurate measurements of surface length for a short crack have been performed at high temperature using a far-field optical microscope. It has been shown that the potential drop technique is inappropriate for these measurements.

The stress intensity factor for a semi-elliptical crack and the crack opening load were determined from FEM modelling using a viscoplastic constitutive set of equations. It has been shown that crack closure effects calculated within the specimen are similar in notched and unnotched specimens except when the crack is close to the notch root.

The typical semicircular shape reached by the crack front can be explained by more important crack closure effects at the free surface than within the specimen. A phenomenological equation has been given to represent this effect in notched bodies. This effect is more pronounced in notched specimens than in unnotched specimens due to the increase of local stress range in the vicinity of the notch. FEM calculations simulating the growth of a 3D fatigue crack from notches are necessary in order to extend these results. Comparison of calculated and observed crack closure effects for short cracks would be useful.

Considering these crack closure calculations, it has been shown that the crack growth rates measured in terms of ΔK_{eff} are the same for short and long cracks. In N18 alloy, the downward trend effect observed during crack propagation can simply be interpreted by a mechanical effect related to crack closure effects.

Acknowledgements

Financial support from SNECMA is greatly acknowledged. Thanks also to Dr J.C. Lautridou from SNECMA and Professor H. Ghonem from University of Rhode Island for many fruitful discussions and to Dr J. Besson for his guidance in numerical modelling.

REFERENCES

1 Suresh, S. and Ritchie, R. O. (1984) Propagation of short fatigue cracks. *Int. Metals Rev.* **29,** 445–476.
2 Pearson, S. (1975) Initiation of fatigue cracks in commercial aluminium alloys and the subsequent propagation of very short cracks. *Engng Fracture Mech.* **7,** 235–247.
3 Lankford, J. (1982) The growth of small fatigue cracks in 7075–T6 aluminium. *Fatigue Fract. Engng Mater. Struct.* **5,** 233–248.
4 Minakawa, K., Newman, J. C. and McEvily, A. J. (1983) A critical study of the crack closure effect on near threshold fatigue crack growth. *Fatigue Fract. Engng Mater. Struct.* **6,** 359–365.
5 Journet, B. G. Lefrancois, A. and Pineau, A. (1989) A crack closure study to predict the threshold behaviour of small cracks. *Fatigue Fract. Engng Mater. Struct.* **12,** 237–246.
6 Elber, W. (1971) The significance of fatigue crack closure. In: *Damage Tolerance in Aircraft Structures*, ASTM STP 486, 1971. American Society of Testing and Materials, Philadelphia, PA, USA, pp. 230–242.
7 Smith, R. A. and Miller, K. J. (1977) Fatigue cracks at notches. *Int. J. Mech. Sci. 19* **1,** 11–22.
8 Leis, B. N. (1985) Displacement controlled fatigue crack growth in inelastic notch fields: implications for short cracks. *Engng Fracture Mech.* **22,** 279–293.
9 Shin, C. S. and Smith, R. A. (1988) Fatigue crack growth at stress concentrations-the role of notch plasticity and crack closure. *Engng Fracture Mech.* **29,** 301–315.
10 Wu, X. R., Newman, J. C., Zhao, W., Swain, M. H., Ding, C. F. and Phillips, E. P. (1998) Small crack growth and fatigue life predictions for high-strength aluminium alloys: Part I- experimental and fracture mechanics analysis. *Fatigue Fract. Engng Mater. Struct.* **21,** 1289–1306.
11 Newman, J. C., Phillips, E. P. and Swain, M. H. (1999) Fatigue-life predictions methodology using small crack theory. *Int. J. Fatigue* **21,** 109–119.
12 Pommier, S., Prioul, C., Lautridou, J. C. and Bompard, P. 1996) Crack closure effect on crack growth rate at 650 °C in double notched specimens of a nickel base superalloy. *Fatigue Fract. Engng Mater. Struct.* **19,** 1117–1128.
13 Pommier, S., Prioul, C. and Bompard, P. (1997) Influence of a negative R ratio on the creep-fatigue behaviour of the N18 nickel base superalloy. *Fatigue Fract. Engng Mater. Struct.* **20,** 93–107.
14 Van Stone, R. H., Gilbert, M. S., Gooden, O. C. and Laflen, J. H. (1988) Constraint loss model for the growth of surface fatigue cracks. In: *Fracture Mechanics*, ASTM STP 969, (Edited by Cruse, T. A.). American Society of Testing and Materials, Philadelphia, PA, USA, pp. 637–656.
15 Wang, X. and Lambert, S. B. (1995) Stress intensity factors for low aspect ratio semi-elliptical surface cracks in finite-thickness

plates subjected to non uniform stresses. *Engng Fract. Mech.* **51,** 517–532.

16 Wang, X. and Lambert, S. B. (1997) Stress intensity factors and weight functions for high aspect ratio semi-elliptical surface cracks in finite-thickness plates. *Engng Fract. Mech.* **57,** 13–24.

17 Pineau, A. (1997) High temperature fatigue of Ni-base superalloys: microstructural and environmental effect. In: *Proceedings of Conference*, '*Engineering against fatigue*', Sheffield, UK, (Edited by J. H. Beynon, M. W. Brown, R. A. Smith, T. C. Lindley and B. Tomkins). A. A. Balkema, Rotterdam, the Netherlands. pp. 557–565.

18 Andrieu, E. and Pineau, A. (1998) Study of the coupled phenomena involved in the oxydation assisted intergranular cracking of Ni based superalloys. In: *Proceeding of the 3rd European Mechanics of Materials Conference 'Mechanics and Multi-Physics Processes in Solids: Experiments, Modelling, Applications'*, Oxford (UK). (Edited by E. Busso and G. Coilletaud). EDP Sciences, Les Ulis, France, pp. 9.3–9.11.

19 Clad, T. (1996) Microstructure and propagation de fissures dans la soudure par friction-inertie de l'alliage N18. Ph.D. Thesis. Paris, France: Ecole des Mines de Paris.

20 Newman, J. C. Jr and Raju, S. R. (1981) An empirical stress-intensity factor equation for the surface crack. *Engng Fracture Mech.* **15,** 185–192.

21 Hochstetter, G. (1994) Propagation des fissures à haute température dans le superalliage N18 pour disques de turbomachine. Interactions entre la nature des sollicitations mecaniques et des effets d'oxydation. Ph.D. Thesis. Paris, France: Ecole des Mines de Paris.

22 Chaboche, J. L. and Lemaitre, J. (1985) *Mécanique des Matériaux Solides.* Paris, France: Dunod, Bordas.

23 Sansoz, F. (2000) Propagation des petites fissures de fatigue dans les zones de concentration de contraintes dans le superalliage N18. Ph.D. Thesis. Paris, France: Ecole des Mines de Paris.

24 Sansoz, F., Brethes, B. and Pineau, A. (1998) Short fatigue crack propagation from notches in N18 Ni based superalloy. In: *ECF12 Conference Proceedings*, Sheffield, UK, Vol. 1, (Edited by M. W. Brown, E. R. de Los Rios and K. J. Miller). Engineering Materials Advisory Services Ltd., Cradley Heath, UK. pp. 61–66.

25 Haigh, J. R. and Skelton, R. P. (1978) A strain intensity approach to high temperature fatigue crack growth and failure. *Mater. Sci. Engng* **36,** 133–137.

26 Fleck, N. A., Smith, I. F. C. and Smith, R. A. (1983) Closure behaviour of surface cracks. *Fatigue Fract. Engng Mater. Struct.* **6,** 225–239.

27 Troha, W. A., Nicholas, T. and Grandt, A. F. (1988) Three-dimensionnal aspects of fatigue crack closure in surface flaws in PMMA material. In: *Mechanics of Wreck Closure*, ASTM STP 982, (Edited by J. C. Newman and W. Elber). American Society of Testing and Materials, Philadelphia, PA, USA, pp. 598–616.

28 Chermahini, R. G., Palmberg, B. and Blom, A. F. (1993) Fatigue crack growth and closure behaviour of semi-circular and semi-elliptical surface flaws. *Int. J. Fatigue* **15,** 259–263.

29 Zhang, J. Z. and Bowen, P. (1998) On the finite element simulation of three-dimensional semi-circular fatigue crack growth and closure. *Engng Fract. Mech.* **60,** 341–360.

30 Newman, J. C. Jr and Armen, H. Jr (1975) Elastic-plastic analysis of a propagating crack under cyclic loading. *AIAA J.* **13,** 1017–1023.

31 Mc Clung, R. C. and Sehitoglu, H. (1989) On the finite element analysis of fatigue crack closure. Part 1 and 2. *Engng Fracture Mech.* **33,** 237–272.

32 Jolles, M. and Tortoriello, V. (1983) Geometry variations during fatigue growth of surface flaws. In: *Fracture Mechanics* 14. ASTM STP 791, (Edited by J. C. Lewis and G. Sines). American Society of Testing and Materials, Philadelphia, PA, USA, pp. I-297–I-307.